RSC Advances

PAPER

View Article Online
View Journal | View Issue

Cite this: *RSC Adv.*, 2017, **7**, 13112

Preparation of dithiocarbamate polymer brush grafted nanocomposites for rapid and enhanced capture of heavy metal ions†

Xin Wang,[a] Shiyao Jing,[a] Yingying Liu,[a] Xiumin Qiu[a] and Yebang Tan*[ab]

Received 31st December 2016
Accepted 19th February 2017

DOI: 10.1039/c6ra28890a

rsc.li/rsc-advances

High-density and narrow-distribution dithiocarbamate (DTC) functionalized polymer brush grafted SiO_2 nanocomposites (DTC-PGMA@SiO_2) were synthesized *via* surface initiated atom transfer radical polymerization (SI-ATRP) and subsequent DTC functionalization, which could serve as an efficient nanostructured adsorbent material. Systematic characterization was performed to identify the sea anemone like core-brush structure. More importantly, the DTC-PGMA@SiO_2 adsorbent exhibited remarkable performance in capturing heavy metal ions from water. The adsorption behaviour, including the effect of pH, adsorption kinetics, adsorption isotherms, adsorption thermodynamics and adsorption mechanism, was investigated in detail. Interestingly, the adsorbent complexes show different color changes depending upon the species of adsorbed ions, indicating that the DTC-PGMA@SiO_2 can be potentially used as a sensor for metallic contaminants in water bodies. The regeneration experiments showed that the adsorbent is both cost-effective and sustainable. The high-capacity and rapid adsorption of metallic ions, which are due to the well-defined core-brush structure, large specific surface area and strong binding ability of DTC groups, make this adsorbent material promising in the capture of heavy metal ions from contaminated water.

Introduction

Water is an essential and significant component of the ecosystem, and plays a vital role in Earth's ecological cycle.[1] Despite this fact, fresh water systems are directly threatened by heavy metal ions contamination.[2–4] Heavy metal ions (such as Pb^{2+}, Cd^{2+}, Cr^{6+}, Hg^{2+}, and Cu^{2+}) can diffuse into surface and ground waters, posing a critical threat to the ecosystem and public health due to their high toxicity, carcinogenicity, non-biodegradability and bioaccumulation in the food chain.[5–8] Common mechanisms regarding the toxicity of heavy metal ions have been reviewed by the World Health Organization (WHO). Some of these include modifying the active conformation of enzymes and proteins, displacing essential metals from biomolecules and disturbing the integrity of biomembranes.[9,10] Consequently, this has led to the development of highly efficient technologies for the removal of heavy metal ions from water bodies.

For this purpose, various methods have been developed over the past few years including ion exchange,[11] chemical precipitation,[12] membrane filtration,[13] reverse osmosis,[14] and adsorption.[15] By contrast, adsorption is considered to be the most suitable process for capturing metallic ions due to its ease of operation, low cost, high efficiency, and safety.[16,17] In order to improve the adsorbent performance, organic chelating ligands have been developed based on imidazole, thiol, dithiocarbamate (DTC), and thiourea, or carbonyl groups.[18,19] It is particularly worth mentioning that the high affinity for metallic ions is a unique characteristic of sulfur containing groups, especially in case of the DTC group.[20–22] DTC group is well-known to be an soft Lewis base, which could form stable complexes with heavy metal ions (soft Lewis acids) containing partially and fully filled d orbitals through π-coordinated interactions.

A large number of adsorbent materials have been designed and studied as heavy metal capturing agents. Some of these include biomass materials,[23] activated carbon,[24] nanoparticles,[25–27] polymer resins,[28] and hydrogels.[29] Compared with other adsorbent materials, nanostructured adsorbent materials exhibit unique properties due to their abundant surface adsorption sites provided by higher specific surface area.[30,31] However, the drawbacks of traditional nano-sized adsorbent materials are also obvious. Some of these drawbacks include

[a]*School of Chemistry and Chemical Engineering, Shandong University, Jinan 250100, People's Republic of China. E-mail: ybtan@sdu.edu.cn*

[b]*The Key Laboratory of Special Functional Aggregated Materials, Ministry of Education, Shandong University, Jinan 250100, People's Republic of China*

† Electronic supplementary information (ESI) available: The synthesis method of sacrificial initiator, bare SiO_2 and Br@SiO_2 nanoparticles, the ^{1}H NMR and FTIR spectra of sacrificial initiator and PGMA (Fig. S1–S4); the kinetic plot of SI-ATRP (Fig. S5); the evolution of M_n and PDI *versus* monomer conversion (Fig. S6); the fitting plots of kinetic and isothermal data (Fig. S7 and S8); the results of reuse experiments (Fig. S9); the elemental analysis results (Table S1), the fitting parameters obtained by using D–R model (Table S2) and the thermodynamic parameters of adsorption process (Table S3). See DOI: 10.1039/c6ra28890a

their natural tendency to agglomerate and the limited monolayer adsorption sites attached to the surface.[32] For this reason, the development of a surface modification to achieve improved and optimized adsorption sites is crucial to the advancement of this field.

Surface functionalization using polymer brush can provide a homogeneous and well-defined interface between nanocomposites and has garnered much attention due to its wide range of applications.[33–35] Additionally, polymers have been used to effectively reduce the agglomeration of nano-sized materials.[36] Being inspired by the structure of sea anemone, which is particularly efficient in capturing plankton, the authors of current study have designed a novel nanostructured adsorbent having a core-brush structure similar to sea anemones. Surface-initiated polymerization (SIP) is a facile means of creating high-density polymer brushes on substrates. More importantly, high-density and well-defined polymer brushes having narrow molecular distribution can be precisely fabricated on the matrix surface by using versatile surface-initiated atom transfer radical polymerization (SI-ATRP).[37–40]

Poly(glycidyl methacrylate) (PGMA), a very valuable polymer, containing active epoxy group that can undergo ring opening reactions with functional ligands. Therefore, the graft of PGMA brush as reactive anchor is of particular interest. Accordingly, adsorptive groups can be introduced to construct efficient adsorptive polymer brush. Surface modification of the adsorptive polymer brushes can not only offer abundant and spatially-organized adsorption sites (just like the tentacles of sea anemones), but can also improve their performance for capturing heavy metal ions. Some previous studies have reported such a modification in the field of adsorption.[41–43] However, few work focused on the fabrication of efficient nanostructured adsorbent materials through SI-ATRP for capturing heavy metal ions.

In this work, a new strategy to design nano-sized heavy metal adsorbent material with core-brush structure is explored by combining SI-ATRP and DTC functionalization. The low-cost bare SiO_2 nanoparticles were initially anchored by ATRP initiator, which was further used for grafting PGMA brushes. Subsequently, the DTC groups were introduced to the polymer brushes through ring-opening reaction and DTC functionalization (see Scheme 1). The resultant nanostructured DTC-PGMA@SiO_2 adsorbent was characterized by various techniques. Moreover, the reported material was finally applied for efficient removal of Cu^{2+}, Pb^{2+} and Cd^{2+} from an aqueous environment. Adsorption behaviours, such as the effect of pH, adsorption kinetics, adsorption isotherms, adsorption thermodynamics and adsorption mechanism were systematically investigated. The regeneration experiments were also conducted to explore the reusability of the studied adsorbent.

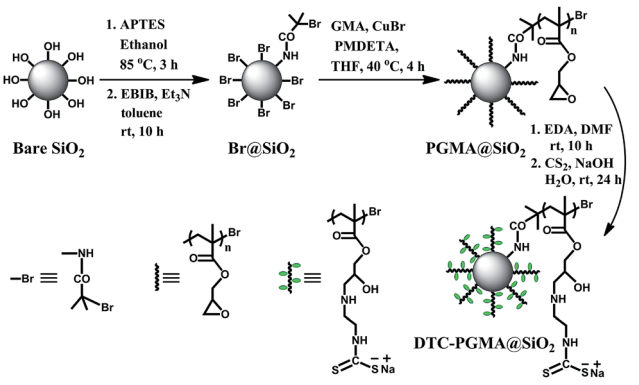

Scheme 1 The synthetic route of nanostructured DTC-PGMA@SiO_2 adsorbent material *via* SI-ATRP and DTC functionalization.

Experimental

Materials and characterization

Chemicals including 3-triethoxysilylpropylamine (APTES), ethylene diamine tetraacetic acid (EDTA), anisole, *N*,*N*-dimethylformamide (DMF), triethylamine (Et_3N), 2-bromoisobutyryl bromide (BiBB), glycidyl methacrylate (GMA), pentamethyldiethylenetriamine (PMDETA), carbon disulfide (CS_2), ethylenediamine (EDA) used are all of analytical grade (J&K Scientific Ltd., Beijing, China). The model sacrificial initiator 2-bromo-2-methyl-*N*-propylpropanamide (BMPA) was self-prepared (see ESI†). Bare SiO_2 nanoparticles and initiator immobilized SiO_2 nanoparticles were prepared according to previous reports (see ESI†).[44] CuBr was successively washed with acetic acid and methanol before use. All of the aqueous solutions were prepared using ultrapure water (18.25 MΩ cm at 25 °C).

The chemical structures of PGMA brush and synthesized materials were determined by ^{1}H NMR (Bruker AVANCE 300 MHz NMR spectrometer) and FT-IR spectra (Bruker Tensor 27 spectrometer). GPC measurements were performed on a Waters 515 GPC system, which used THF as the eluent (flow rate 1 mL min^{-1}). TGA was measured by a Netzsch STA 449 instrument from 40 °C up to 800 °C. The morphology observations of materials were observed with a Hitachi S4800 scanning electron microscope (SEM) and a JEM 1011 transmission electron microscope (TEM). Water contact angle measurements were performed using a Kruss DSA10 optical contact angle system. Elemental analysis of C, H, N and S was carried out by using an Elementar Vario Cube EL analyser. XPS spectra were acquired by using a Perkin Elmer PHI5300 spectrometer. Zeta potential measurements of adsorbent suspensions (0.2 g DTC-PGMA@SiO_2 in 50 mL of 0.1 mol L^{-1} NaCl solution) were carried out by a Malvern Zetasizer Nano ZS90 system. The concentrations of metal ions in the solution were determined by inductively coupled plasma-atomic emission spectrometer (ICP-AES, Thermo Optima 7000DV).

Growth of PGMA brushes on Br@SiO_2 nanoparticles

The surface of prepared Br@SiO_2 nanoparticles can provide abundant initiators for triggering the graft of PGMA brushes through SI-ATRP, during which CuBr/PMDETA (in 1 : 1 molar ratio, respectively) was used as the catalyst. 4 g Br@SiO_2, GMA (20 mL; 146.32 mmol), BMPA (101.5 mg; 0.487 mmol) and PMDETA (100 μL; 0.487 mmol) were dissolved in 30 mL anisole. The solution was processed by several freeze–pump–thaw cycles to remove oxygen. CuBr (70 mg; 0.487 mmol) was ultrasonically dispersed in the reaction flask under N_2 atmosphere. The

system was initiated at 40 °C, and the polymerization was stopped after 5 h by opening the flask. The PGMA brushes grafted SiO_2 nanocomposites (PGMA@SiO_2) were purified by THF washing, EDTA (0.05 mol L^{-1} solution) washing, acetone washing and vacuum drying. The free PGMA brushes were precipitated in acetone and were purified through a column of neutral alumina using THF as eluent.

DTC functionalization of PGMA@SiO_2 nanocomposites

4 g PGMA@SiO_2 were dispersed and stirred in 50 mL 4 mol L^{-1} EDA/DMF solution for 10 h at room temperature. The generated amino functionalized PGMA@SiO_2 (NH_2-PGMA@SiO_2) nanocomposites were washed thoroughly with acetone and then, were dried under vacuum. 4 g of prepared NH_2-PGMA@SiO_2 were dispersed in 40 mL of 2 mol L^{-1} NaOH aqueous solution. After the addition of 2 mL CS_2, the mixture was stirred at room temperature for 24 h. The target DTC-functionalized PGMA@SiO_2 (DTC-PGMA@SiO_2) adsorbent nanocomposites were thoroughly and successively washed with water and acetone, and then, were dried under vacuum.

Metallic ions adsorption tests

All adsorption experiments were performed in batch mode and using a constant temperature incubator shaker (Julabo SW-22) at 150 rpm. The effect of pH (within the range of 1.0–7.0) was investigated in NaAc-HAc buffer solutions having an initial metal ion concentration of 800 mg L^{-1}. The temperature was kept constant at 25 °C during each 150 minute long adsorption experiment. For kinetic studies, the experiments were carried out at pH = 5.0 with different adsorption time intervals (from 3 to 150 min) at 25 °C, where the initial concentration of the investigated metallic ion was 800 mg L^{-1}. The adsorption isotherms were investigated at pH = 5.0 by varying the initial concentration of heavy metal ions within the range of 200–2000 mg L^{-1}. Furthermore, all isothermal experiments were conducted at three different temperatures (298 K, 308 K and 318 K) to investigate the adsorption thermodynamic parameters. The adsorption capacity (Q_e; mmol g^{-1}) and removal efficiency (R; %) were calculated using eqn (1) and (2), respectively.

$$Q_e = V \times (C_0 - C_e)/m \quad (1)$$

$$R = (C_0 - C_e)/C_0 \times 100\% \quad (2)$$

where C_0 and C_e represent the initial and equilibrium concentrations of the metallic ions (mmol L^{-1}), respectively; V is the volume of the solution (20 mL), and m is the mass of adsorbent dosage (20 mg).

Regeneration of DTC-PGMA@SiO_2 adsorbent

The adsorbent loaded with heavy metal ions was immersed in 0.2 mol L^{-1} HNO_3 solution for 2 h. Next, the adsorbent was successively washed with 0.1 mol L^{-1} EDTA solution, deionized water and acetone. After the centrifugal separation at 11 000 rpm for 5 min, the regenerated DTC-PGMA@SiO_2 nanocomposite was dried under vacuum. The adsorption performance of regenerated DTC-PGMA@SiO_2 nanocomposite was evaluated in heavy metal ion solution having an initial concentration of 200 mg L^{-1} (the adsorption was performed as above-mentioned isothermal adsorption experiment at 25 °C, pH = 5.0).

Results and discussion

FTIR analysis

Each step in the preparation of DTC-PGMA@SiO_2 adsorbent was monitored by FTIR spectra (see Fig. 1). The strong adsorption band at 1103 cm^{-1} was assigned to Si–O–Si stretching vibration of SiO_2 substrate. For Br@SiO_2, the appearance of adsorption bands at 1652 cm^{-1} and 1553 cm^{-1} represented the amide condensation reaction between NH_2@SiO_2 and BiBB. Moreover, the appearance of weak C–Br band at 550 cm^{-1} also demonstrated the BiBB immobilization on SiO_2. Compared with Br@SiO_2, the PGMA@SiO_2 showed strong adsorption peaks at 2998 and 2988 cm^{-1}, which were attributed to aliphatic C–H stretching vibration of PGMA brushes. In addition, the characteristic signals for GMA at 910 (epoxy group) and 1731 cm^{-1} (carbonyl stretching vibration of the ester group) were observed.[45] For NH_2-PGMA@SiO_2, both the disappearance of characteristic peak for epoxy group and the appearance of adsorption bands at 3368, 3286 and 1475 cm^{-1} (N–H stretching vibration of primary amino group and C–N stretching vibration) represented the introduction of amino groups *via* an exhaustive ring-opening reaction between PGMA and EDA. The spectrum of DTC-PGMA@SiO_2 showed remarkable characteristic signals for DTC group at 1490 (N–CS_2 vibration), 985 (C–S vibration) and 1160 cm^{-1} (C=S vibration),[22] indicating that the DTC groups have been successfully introduced in the polymer brushes.

XPS determination and elemental analysis of nanocomposites

The XPS spectra of NH_2@SiO_2, Br@SiO_2, PGMA@SiO_2 and DTC-PGMA@SiO_2 have been shown in Fig. 2. The peaks of Si 2p, Si 2s, C 1s, N 1s and O 1s were identified in the NH_2@SiO_2 spectrum. The survey spectrum of Br@SiO_2 confirms the presence of Br (Br 3d

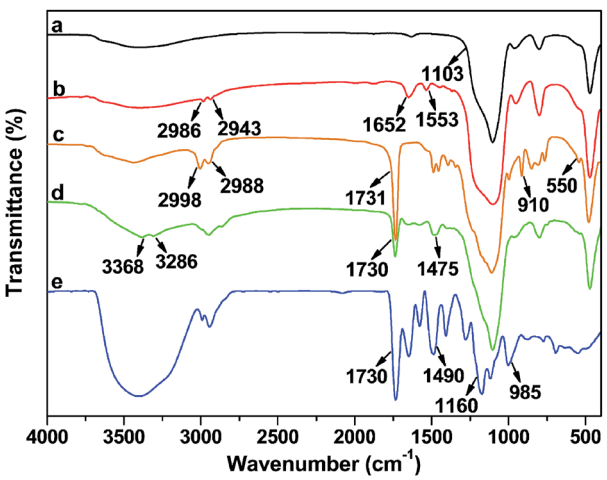

Fig. 1 FTIR spectra of bare SiO_2 (a), Br@SiO_2 (b), PGMA@SiO_2 (c), NH_2-PGMA@SiO_2 (d) and DTC-PGMA@SiO_2 (e) samples.

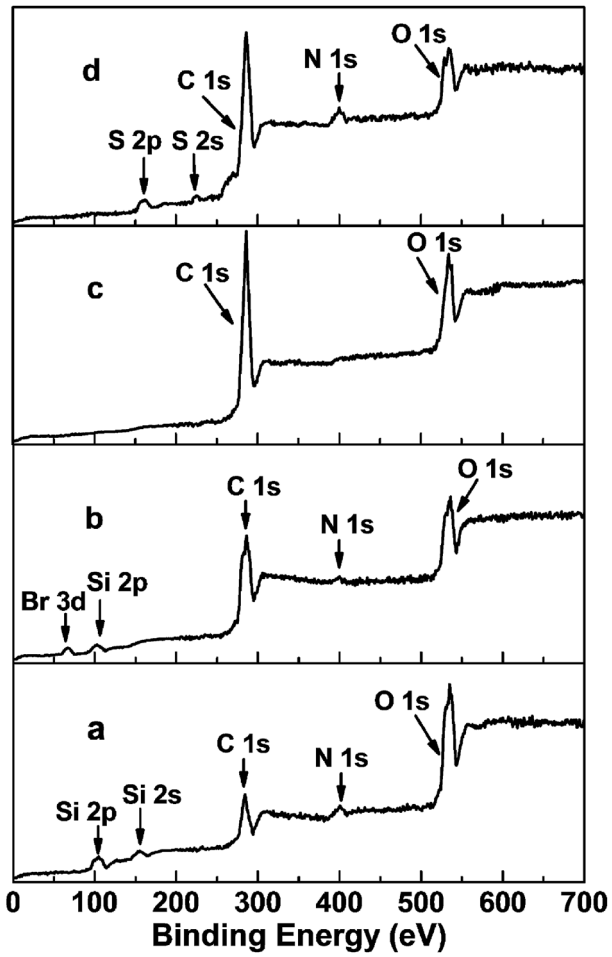

Fig. 2 XPS survey spectra of NH_2@SiO_2 (a), Br@SiO_2 (b), PGMA@SiO_2 (c) and DTC-PGMA@SiO_2 (d) samples.

peak at about 69 eV).[46] For PGMA@SiO_2, the remarkable increase in the intensity of C 1s and the disappearance of Si 2p, Si 2s and Br 3d peaks implied that the high-density PGMA brushes were grafted on the surface of SiO_2 nanoparticles. The signals of S 2s and N 1s in the XPS spectrum of DTC-PGMA@SiO_2 further confirmed the introduction of DTC groups. The elemental analysis results (in Table S1†) showed the content of C increased significantly due to the grafting of PGMA. The N content was strongly enhanced by the ring-opening reaction occurring between GMA and EDA. The drastic increase of S content from zero to 32.38% confirmed the introduction of abundant DTC groups (according to sulphur content, the calculated quantity of DTC group is 6.52 mmol g^{-1}).

Molecular structure characterization of PGMA brushes

The synthesized model sacrificial initiator BMPA has very similar initiating chemical structure with the grafted-initiator (see Fig. S1–S3†). It is widely accepted that the ATRP initiated by the model sacrificial initiator shows almost similar polymerization behaviour as the SI-ATRP performed on a solid support.[47–49] Therefore, the obtained free polymer brushes were generally used to evaluate the control of SI-ATRP experiments. The chemical structure of PGMA brushes was confirmed by ^1H NMR (see Fig. S4†). The GPC traces of free PGMA brushes with various [GMA] : [BMPA] : [CuBr] : [PMDETA] ratios were detected (see Fig. 3), wherein the molecular weight and polydispersity were found to decrease with the increasing initiator content. As shown in Fig. S5,† the kinetic data of polymerization ([GMA] : [BMPA] : [CuBr] : [PMDETA] is [300] : [1] : [1] : [1]) was found to follow the first-order kinetic model. Fig. S6† displayed the evolution of M_n and PDI with the monomer conversion. It was found that the M_n of PGMA brush increased linearly with the increase of GMA monomer conversion. Additionally, the narrow PDI values illustrated that the SI-ATRP experiments were well-controlled, and therefore well-defined PGMA brushes were expected to be fabricated on the substrate surface. Ultimately, $PGMA_3$ brushes having the highest molecular weight were selected to perform the present research.

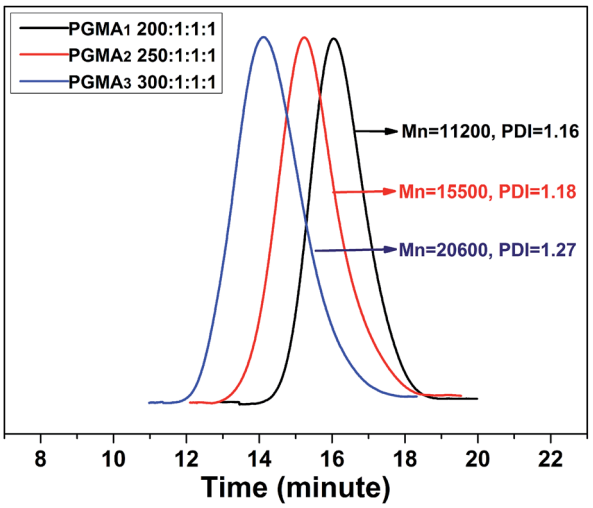

Fig. 3 GPC traces of free PGMA brushes synthesized at different [GMA] : [BMPA] : [CuBr] : [PMDETA] molar ratio.

TGA measurements of nanocomposites

TGA is one of the most appropriate methods to evaluate the thermal stability and graft ratios of the materials.[50] As shown in Fig. 4, the weight loss increased stage-by-stage from bare SiO_2 substrate to DTC-PGMA@SiO_2. A significant weight loss in PGMA@SiO_2 (*ca.* 62.4%) was observed after 240 °C, which demonstrated a high-density grafting of PGMA brushes. Both NH_2-PGMA@SiO_2 and DTC-PGMA@SiO_2 displayed another thermal decomposition at around 320 °C, which implied that a new chemical structure has emerged following the ring-opening reaction. The final weight loss ratios of NH_2-PGMA@SiO_2 and DTC-PGMA@SiO_2 were found to be 76.2% and 84.2%, respectively. These results indicated complete evolution of ring opening reaction and DTC functionalization.

Morphology observations of nanocomposites

TEM micrographs of bare SiO_2, PGMA@SiO_2 and DTC-PGMA@SiO_2 are displayed in Fig. 5a–c respectively. Compared with the bare SiO_2, the PGMA@SiO_2 clearly showed the grafted polymer brushes, while the agglomeration of nanocomposites

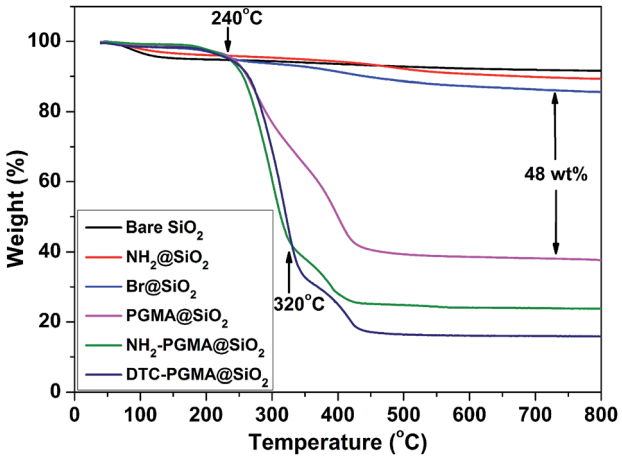

Fig. 4 TGA curves of synthesized nanocomposites.

turned obvious. This is due to the reason that water is a poor solvent for PGMA. So, the brushes curl to form links between PGMA@SiO_2 nanocomposites in water, which exacerbate the agglomeration. After the DTC modification, all of the nanocomposites in water seemed to be finely dispersed and appeared to be much bigger than before (the size of DTC-PGMA@SiO_2 is about 200 nm in water). This is due to the reason that the negatively charged DTC-modified polymer brushes exhibit super hydrophilicity. Besides, these have electrostatic repulsions in between them. Accordingly, these brushes become stretched in water and hence, the dispersibility of nanocomposites is remarkably improved. In this form, the DTC-PGMA@SiO_2 adsorbent exhibits unique advantages to capture heavy metal ions from aqueous environments.

Measurement of water contact angle of nanocomposites

Materials generally show significant difference in wettability following surface modification.[51,52] The wettability of sample disks including SiO_2, PGMA@SiO_2 and DTC-PGMA@SiO_2 (Fig. 5d–f, respectively) was assessed. For bare SiO_2, the Si–OH groups make the surface hydrophilic (water contact angle of around 28°). However, the majority of Si–OH groups are consumed during the condensation reaction involving Si–OC_2H_5 groups of APTES. Additionally, the grafting of high-density hydrophobic PGMA brushes leads to a much more hydrophobic surface of PGMA@SiO_2 (water contact angle of around 87°). However, the water drops were found to readily wet the surface of DTC-PGMA@SiO_2 disk. A transition to a super hydrophilic surface is observed on the DTC-PGMA@SiO_2 disk as the contact angle decreases to 9°. Thus, the changes in wettability and TEM observations provide useful complementary information, testifying that the design of nanostructured DTC-PGMA@SiO_2 adsorbent occurred as expected.

Effect of pH on adsorption

The surface charge of the adsorbent, ionization of functional groups and speciation of heavy metal ions are strongly affected by the pH of environment. Consequently, the pH effect on the removal of heavy metal ions using DTC-PGMA@SiO_2 was investigated. As shown in Fig. 6a, poor uptake of metallic ions was observed in strongly acidic environment (pH < 3.0), while it increased remarkably for a higher pH value. The maximum uptake of Cu^{2+}, Pb^{2+} and Cd^{2+} (3.45, 1.97 and 1.56 mmol g^{-1}, respectively) was observed at a pH of 5.0. To elaborate this phenomenon, the pH point of zero charge (pH_{PZC}) of the nanostructured DTC-PGMA@SiO_2 adsorbent was measured *via* zeta

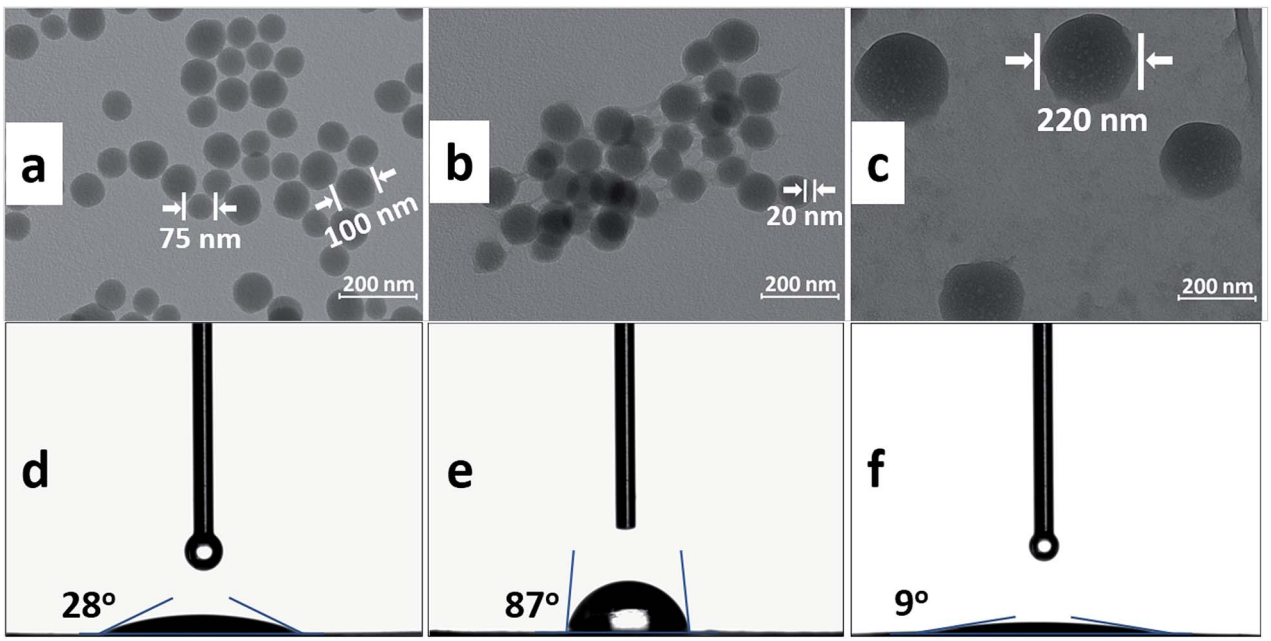

Fig. 5 TEM images of bare SiO_2 nanoparticles (a), PGMA@SiO_2 (b) and DTC-PGMA@SiO_2 (c) dispersed in water. Water contact angle measurements on bare SiO_2 (d), PGMA@SiO_2 (e) and DTC-PGMA@SiO_2 (f) sample disks are shown.

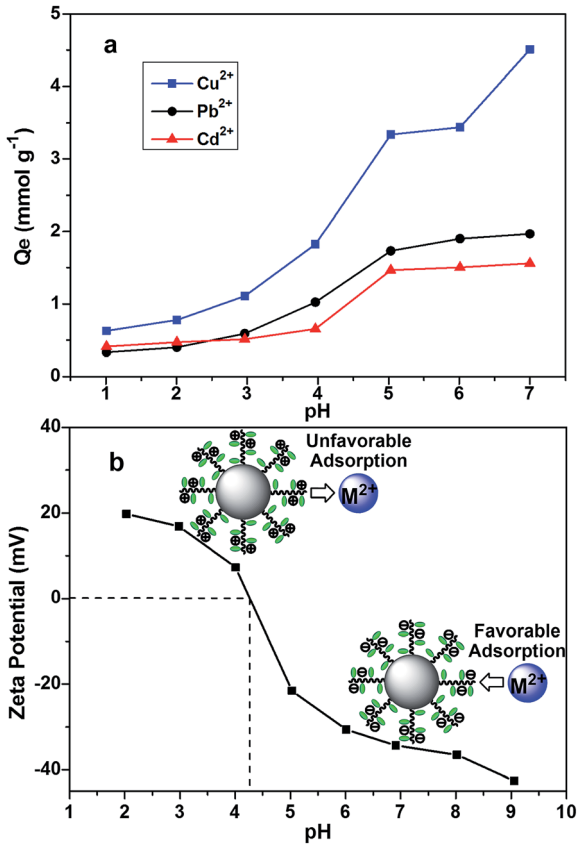

Fig. 6 (a) Adsorption capacity as a function of the pH for the studied metal ions. (b) Zeta potential of the DTC-PGMA@SiO_2 suspension as a function of the pH.

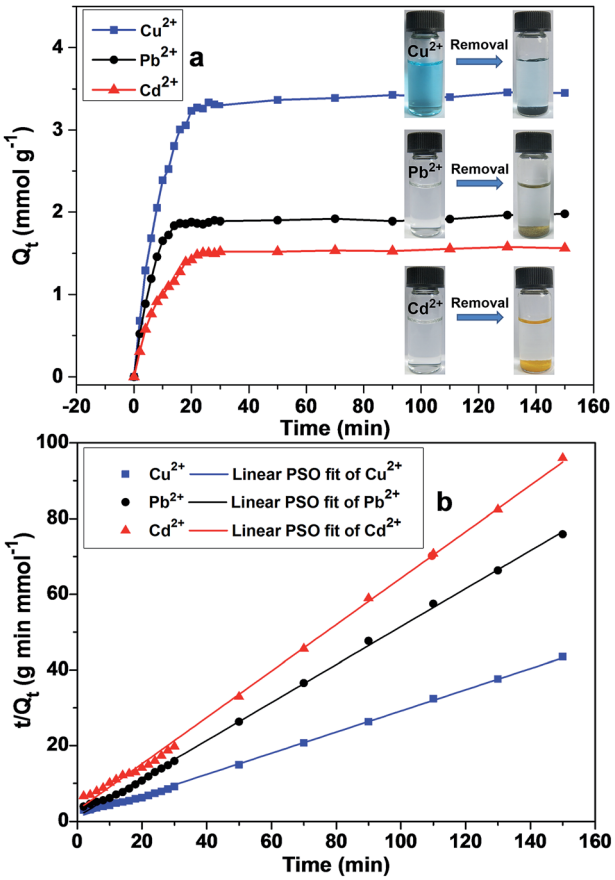

Fig. 7 (a) Adsorption kinetics of metal ions on DTC-PGMA@SiO_2 at 298 K. (b) Linear fitting plots of kinetic data using a pseudo-second-order model.

potential method (see Fig. 6b). The pH_{PZC} was found to be about 4.3. It is well-known that the adsorbent surface is positively charged at pH < pH_{PZC}, while it is negatively charged at pH > pH_{PZC}.[53,54] Under low pH conditions (pH < pH_{PZC}), the functional groups (amine and DTC groups on the polymer brushes) were protonated, indicating that abundant H^+ ions would dominantly compete with heavy metal ions for binding these adsorptive sites. Conversely, the removal of metallic ions was facilitated significantly with an increase in the pH value. However, the generation of precipitates of metallic hydroxides obviously disturbed the accurate evaluation of adsorption capacity at higher pH values (pH $\geq$ 6.0). Therefore, pH = 5.0 was chosen to perform further experiments to study the adsorption behaviour.

Adsorption kinetics

In order to investigate the performance of DTC-PGMA@SiO_2 adsorbent, the adsorption kinetics for metallic ions (including Cu^{2+}, Pb^{2+} and Cd^{2+}) were examined. As shown in Fig. 7a, the time to reach equilibrium was found to be less than 30 min for the investigated ions. Such a rapid adsorption is ascribed to the large specific surface area and the strong metal affinity of DTC groups. Remarkably, for Pb^{2+}, the adsorption equilibrium time is only about 15 min. This is due to the smaller ionic radius of hydrated Pb^{2+} (4.01 Å) compared to those of Cu^{2+} (4.19 Å) and Cd^{2+} (4.26 Å),[55,56] resulting in an easier diffusion of Pb^{2+} to the adsorption sites.[22,57] In order to further understand the mechanism of adsorption process, linear pseudo-first-order (PFO) and pseudo-second-order (PSO) models were used to fit the kinetic data. The governing equations for the models are given by eqn (3) and (4), respectively.[43,58]

$$\ln(Q_e - Q_t) = \ln Q_e - k_1 t \quad (3)$$

$$t/Q_t = 1/(k_2 Q_e^2) + t/Q_e \quad (4)$$

where Q_e and Q_t (mmol g^{-1}) are the amounts of adsorbed metal ions at equilibrium and at test time t (min), respectively. In eqn (3) and (4), k_1 (min^{-1}) and k_2 (g $mmol^{-1}$ min^{-1}) are the relevant rate constants.

Linear fitting plots were shown in Fig. 7b (fitting plots using PFO model were shown in Fig. S7†) and the corresponding fitting parameters were reported in Table 1. According to R^2 values, PSO represented the experimental data better than the PFO model. These results demonstrated that the adsorption process of metallic ions onto the DTC-PGMA@SiO_2 adsorbent could well be explained by the pseudo-second-order kinetic model. This also indicated that the rate-limiting step should be the chemisorption of adsorbate on the adsorbent represented by the valence force through an exchange of electrons between DTC ligands and metallic ions.[22,56] It is interesting to note that

Table 1 Kinetic data obtained by PFO and PSO models for the adsorption of heavy metal ions on the nanostructured DTC-PGMA@SiO_2 adsorbent at 298 K

		Fitting parameters		
Model	Metal ion	R^2	Q_e (mmol g^{-1})	K_1 (min^{-1})
PFO	Cu^{2+}	0.298	10.11	0.0011
	Pb^{2+}	0.194	11.02	0.0037
	Cd^{2+}	0.314	11.51	0.0042
		Fitting parameters		
Model	Metal ion	R^2	Q_e (mmol g^{-1})	K_2 (mmol g^{-1} min^{-1})
PSO	Cu^{2+}	0.998	3.57	0.167
	Pb^{2+}	0.999	1.99	0.203
	Cd^{2+}	0.998	1.60	0.131

the chelate complexes show different colour changes depending upon the adsorbed ions (see Fig. 7a), which due to the charge transfer between ligand and metal ions.[59] Consequently, DTC-PGMA@SiO_2 can be used as a potential sensor to identify the contaminating ions in water.

Adsorption isotherms

The study of adsorption isotherms gives a more profound understanding of the adsorbent's performance. Fig. 8 displayed the adsorption isotherms of Cu^{2+}, Pb^{2+} and Cd^{2+} on the nanostructured DTC-PGMA@SiO_2 at 298 K. It can be seen that the uptake of heavy metal ions showed a steeper curve at low concentrations, which gradually reached a plateau at higher concentrations. The adsorption of Cu^{2+} (3.60 mmol g^{-1}) was found to be higher than those of Pb^{2+} (1.96 mmol g^{-1}) and Cd^{2+} (1.47 mmol g^{-1}). The Langmuir and Freundlich empirical isotherm models were fitted to the experimental data. The Langmuir isotherm describes the adsorption on a homogeneous surface, assuming equal adsorption sites, a monolayer surface coverage of adsorbate and no interaction between the adsorbed ions.[59] The Freundlich model depicts an adsorption on a heterogeneous surface, possessing discriminatory adsorption sites and a binding affinity which decreases with the increase in adsorption degree.[60] The Langmuir and Freundlich isotherms are represented by eqn (5) and (6), respectively.

$$C_e/Q_e = C_e/Q_m + 1/Q_m K_L \quad (5)$$

$$\ln Q_e = \ln K_F + 1/n \ln C_e \quad (6)$$

where Q_e (mmol g^{-1}) is the adsorption capacity, Q_m (mmol g^{-1}) is the maximum adsorption capacity, C_e (mmol L^{-1}) is the equilibrium concentration of heavy metal ion in the solution, K_F is a constant reflecting the binding affinity and K_L is the Langmuir adsorption equilibrium constant.

The corresponding results for the fit of Langmuir and Freundlich models have been shown in Fig. 8 and S8,† respectively. Comparing the R^2 values in Table 2, Langmuir model shows better fit for the experimental data, which demonstrates that the adsorption of metal ions on the DTC-PGMA@SiO_2 adsorbent is a monolayer, chemisorption onto a homogeneous surface. The Dubinin–Radushkevitch (D–R) eqn (7) was used to further describe the metal ions' adsorption process.

$$\ln Q_e = \ln Q_m - k\varepsilon^2 \quad (7)$$

where k (mol^2 kJ^{-2}) is a constant related to the average adsorption energy (E) and ε is equal to $[RT \ln(1 + 1/C_e)]$. Furthermore, the E value can be calculated from the k value using eqn (8).

$$E = (2k)^{-1/2} \quad (8)$$

In the present work, E values for the studied metallic ions were found to lie within a range of 18–23 kJ mol^{-1} (see Table S2†). This suggests that a strong binding interaction occurs during the adsorption process rather than a simple ion exchange. DTC is well-known to be an anionic dithio ligand, which could form stable complexes with heavy metal ions containing partially and fully filled d orbitals through π-coordinated interactions. From the ligand field stabilization energy theory, d^9 type metal ions (such as Cu^{2+}) have stronger stabilization energy with respect to d^{10} type ions (such as Pb^{2+} and Cd^{2+}) and therefore, a more significant coordination interaction can be achieved for Cu^{2+}.[61] Differences in the adsorption of Pb^{2+} and Cd^{2+} mainly rely on their electronegativity, which are 2.33 for Pb and 1.7 for Cd. The higher electronegativity of Pb reflects its higher tendency to share electrons with respect to Cd, thus favouring its adsorption on DTC-PGMA@SiO_2 adsorbent.[22] Therefore, the capacity of DTC-PGMA@SiO_2 adsorbent for

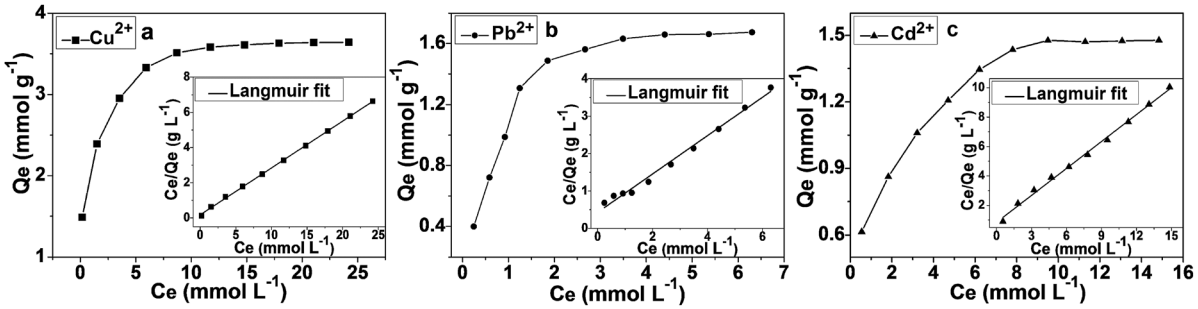

Fig. 8 Adsorption isotherms and relative Langmuir linear fits for the adsorption of Cu^{2+} (a), Pb^{2+} (b) and Cd^{2+} (c) on DTC-PGMA@SiO_2 at 298 K.

Table 2 Isothermal parameters obtained by using Langmuir and Freundlich models for the adsorption of heavy metal ions on the nanostructured DTC-PGMA@SiO_2 adsorbent at 298 K

		Fitting parameters		
Model	Metal ion	R^2	Q_m (mmol g^{-1})	K_L (L $mmol^{-1}$)
Langmuir	Cu^{2+}	0.999	3.75	1.526
	Pb^{2+}	0.990	1.94	0.991
	Cd^{2+}	0.996	1.64	0.727
		Fitting parameters		
Model	Metal ion	R^2	n	K_F ($mmol^{1-1/n}$ $L^{1/n}$ g^{-1})
Freundlich	Cu^{2+}	0.921	5.39	2.19
	Pb^{2+}	0.853	2.20	0.90
	Cd^{2+}	0.935	3.52	0.75

capturing the studied metallic ions can be represented as Cu^{2+} > Pb^{2+} > Cd^{2+}. The results showed that the reported DTC-PGMA@SiO_2 adsorbent shows an outstanding adsorption performance including remarkable adsorption capacity and rapid adsorption rate, which due to the sea anemone like core-brush structure, the strong binding affinity between metal ions and DTC ligand and the high specific area. The comparison between DTC-PGMA@SiO_2 nanocomposite and some other nanomaterials regarding to the adsorption performance of Cu^{2+}, Pb^{2+} and Cd^{2+} from aqueous environment was listed in Table 3.

Adsorption thermodynamics

Adsorption thermodynamics were investigated through temperature-dependent isotherms (see Fig. 9a–c). Van't Hoff equation, as given by eqn (9), is used to calculate the adsorption Gibbs free energy (ΔG; kJ mol^{-1}), adsorption enthalpy (ΔH; kJ mol^{-1}) and adsorption entropy (ΔS; J mol^{-1} K^{-1})

$$\ln K_c = -\Delta H/RT + \Delta S/R \quad (9)$$

where K_c is the adsorption equilibrium constant obtained from Langmuir isotherms at various temperatures, R is the ideal gas constant (8.314 J mol^{-1} K^{-1}), and T is the absolute temperature (K).

The values of ΔH and ΔS can be geometrically extracted from the linear fit of ln K_c *versus* $1/T$ (as shown in Fig. 9d). ΔG can be calculated from ΔH and ΔS values by using eqn (10).

$$\Delta G = \Delta H - T\Delta S \quad (10)$$

The thermodynamic parameters for the studied metallic ions are tabulated in Table S3.† Since ΔG values are more negative at higher temperatures, therefore the spontaneous adsorption is favoured by high temperatures. Positive ΔH values indicate an endothermic adsorption process.[67] The calculated ΔS values also demonstrate that the adsorption process is favoured by the entropy.

Adsorption mechanism

The adsorption mechanism of heavy metal ions using DTC-PGMA@SiO_2 adsorbent is relied on synergistic combination of electrostatic interaction (between metallic ions and functional groups such as amino and DTC groups) and some other stronger chemical interactions. On the basis of hard and soft acids and bases theory, the adsorption may be dominated by the coordination interaction between metal ions and DTC groups. In order to confirm this, FTIR and high-resolution XPS analysis of Cu^{2+}/DTC-PGMA@SiO_2 complex were performed. The red-shift and the intensity reduction of characteristic FTIR DTC signals (C–S and C=S stretching vibrations) following the adsorption of Cu^{2+}, clearly demonstrated that the coordination interactions between Cu^{2+} and DTC groups actually occurred (see Fig. 10a). In XPS spectrum of Cu 2p (see Fig. 10b), Cu $2p_{3/2}$ (932.5 eV) and Cu $2p_{1/2}$ (952.2 eV) peaks were identified, indicating the presence of Cu(II).[68] The S $2p_{3/2}$ (161.9 eV) and S $2p_{1/2}$ (163.3 eV) peak doublet contributed to the unique DTC sulphur signal (see Fig. 10c), which is consistent with the reported DTC–metal ion interaction.[68–70] Additionally, the highly coloured chelate complex and the discussed adsorption preference could be regarded as other proofs. By comparing the FTIR spectra and S 2p XPS signal of

Table 3 Comparison of the adsorption performance of DTC-PGMA@SiO_2 nanocomposite and some other nanomaterials

	Adsorption capacity (mmol g^{-1})					
Adsorbent materials	Cu^{2+}	Pb^{2+}	Cd^{2+}	Equilibrium time (min)	pH conditions	Reference
Polyvinyltetrazole grafted resin	2.65	1.52	—	90–120	5.0	43
Magnesium titanate nanorod	—	1.16	—	10	5.0	53
Mesoporous organosilica embedded with carbon dots	1.72	0.68	—	30	7.0	56
Graphene oxide membrane	1.14	—	0.75	20	5.7	62
PVA/graphene oxide nanofiber	0.51	—	0.40	30	5.8	63
Graphene oxide functionalized with ethylenediamine triacetic acid	1.71	2.19	—	30	3.0 for Pb^{2+}; 5.0 for Cu^{2+}	64
Hydrogel-supported nanosized hydrous manganese dioxide	0.857	0.972	0.835	150	5.0 for Cu^{2+}; 5.0 for Pb^{2+}; 5.5 for Cd^{2+}	65
Soy protein hollow microsphere	1.02	0.62	0.74	240	5.5	66
DTC-PGMA@SiO_2	3.60	1.95	1.47	10–30	5.0	Present work

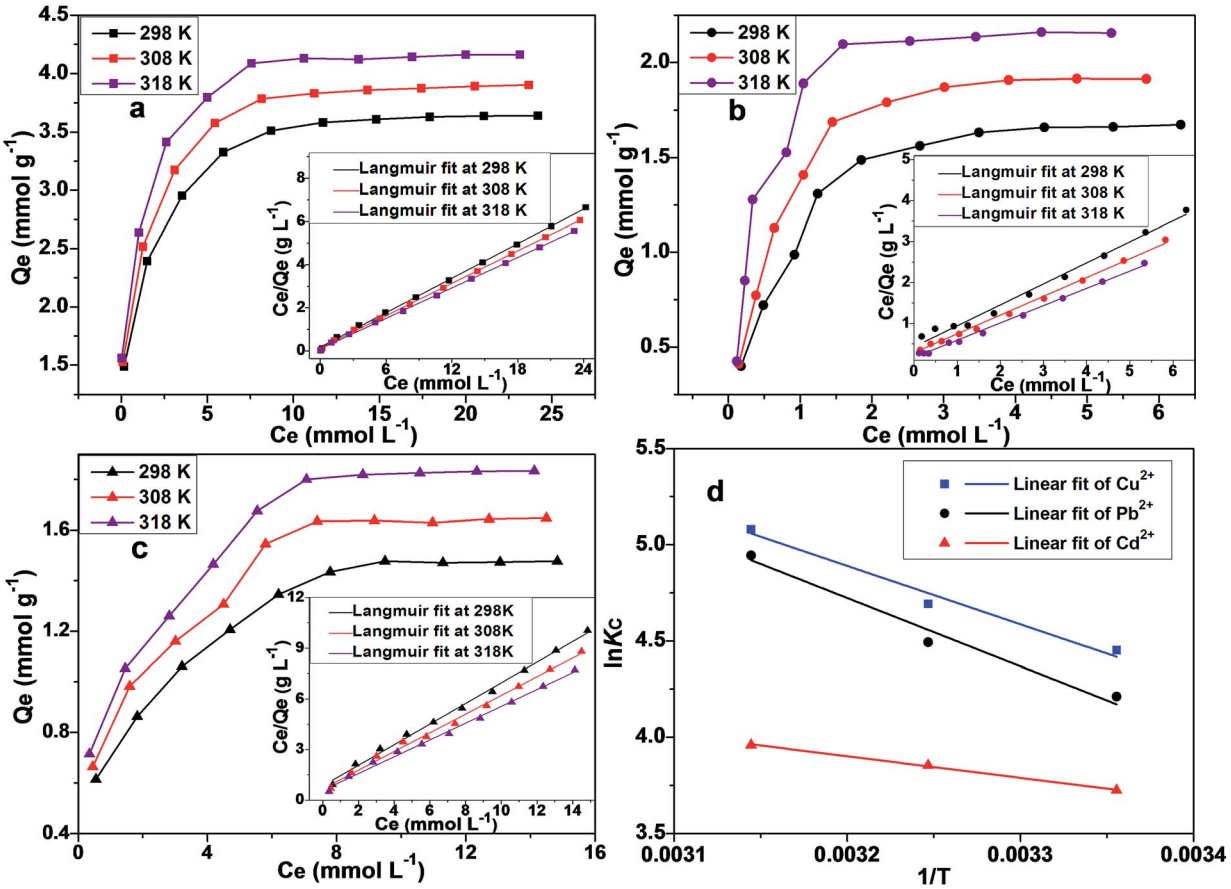

Fig. 9 Adsorption isotherms and Langmuir linear fits for the adsorption of Cu^{2+} (a), Pb^{2+} (b) and Cd^{2+} (c) at 298 K, 308 K and 318 K. (d) The linear fitting plots for ln K_c *versus* 1/*T* according to Van't Hoff equation.

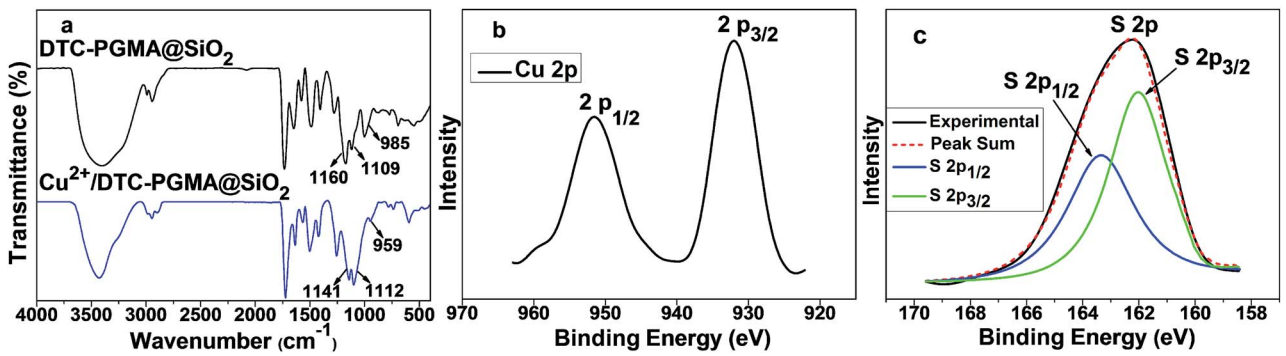

Fig. 10 (a) FTIR spectra of DTC-PGMA@SiO_2 adsorbent and the Cu^{2+}/DTC-PGMA@SiO_2 complex. High-resolution XPS data of Cu 2p (b) and S 2p (c) signals of the Cu^{2+}/DTC-PGMA@SiO_2 complex.

Cu^{2+}/DTC-PGMA@SiO_2 complex, Pb^{2+}/DTC-PGMA@SiO_2 complex and Cd^{2+}/DTC-PGMA@SiO_2 complex, we found no significant differences. Therefore, the adsorption mechanism of the investigated heavy metal ions using DTC-PGMA@SiO_2 adsorbent can be summarized as a unified principle. To summarize, these results confirmed that the metallic ions can be adsorbed on DTC-PGMA@SiO_2 *via* electrostatic interaction and coordination interaction with DTC groups.

Regeneration of DTC-PGMA@SiO_2 adsorbent

The regeneration features of DTC-PGMA@SiO_2 adsorbent for repeated use were investigated. The pH factor has obviously been taken into account, due to which, the pH has proven to be a remarkable influencing factor in the binding interactions between DTC groups and metallic ions. Because of the significant chelating ability of EDTA, it was also used to further improve the metallic ions' desorption from the adsorbent. After four reuse

cycles, the removal efficiencies for Cu^{2+}, Pb^{2+} and Cd^{2+} were 85.7%, 84.3% and 63.5% respectively, which decreased slightly compared with the corresponding values for the first cycle (see Fig. S9†). These results demonstrated that an effective regeneration of DTC-PGMA@SiO_2 can be achieved, which makes it sustainable and economically valuable adsorbent for wastewater treatment.

Conclusions

In summary, a novel nanostructured DTC-PGMA@SiO_2 adsorbent material containing well-defined core-brush structure was synthesized *via* SI-ATRP and subsequent DTC group functionalization. The high-density (grafting ratio is 62.4%) and narrow-distribution polymer brushes, which contain abundant DTC groups (6.52 mmol g^{-1}), were identified by combining multiple techniques. The nanostructured DTC-PGMA@SiO_2 adsorbent exhibits remarkable adsorption performance for d^9 and d^{10} type heavy metal ions, including considerable adsorption capacities (the adsorption capacities for Cu^{2+}, Pb^{2+} and Cd^{2+} were found to be 3.60, 1.96 and 1.47 mmol g^{-1}, respectively) and rapid adsorption equilibriums (within 30 min), which were attributed to the sea anemone-like core-brush structure, large specific surface area and high affinity between DTC groups and metallic ions. The adsorption process can be well-described by the pseudo-second-order and Langmuir models, indicating a spontaneous monolayer chemisorption occurring on the adsorbent surface. The adsorption mechanism between metal ions and DTC-PGMA@SiO_2 adsorbent relies on synergistic combination of electrostatic interaction and coordination interaction between heavy metal ions and DTC groups. Additionally, the effective regeneration was achieved. These results highlight the promising potential of DTC-PGMA@SiO_2 for treating water bodies contaminated by heavy metal ions.

Acknowledgements

The authors are grateful for financial support from the National Natural Science Foundation of China (Grant No. 21374055) and the Major Research of Science and Technology, China (Grant No. 2016ZX05025-003).

Notes and references

1 C. J. Vörösmarty, P. B. McIntyre, M. O. Gessner, D. Dudgeon, A. Prusevich, P. Green, S. Glidden, S. E. Bunn, C. A. Sullivan, C. R. Liermann and P. M. Davies, *Nature*, 2010, **467**, 555–561.
2 Q. Peng, J. Guo, Q. Zhang, J. Xiang, B. Liu, A. Zhou, R. Liu and Y. Tian, *J. Am. Chem. Soc.*, 2014, **136**, 4113–4116.
3 W.-H. Leung, P.-K. So, W.-T. Wong, W.-H. Lo and P.-H. Chan, *RSC Adv.*, 2016, **6**, 106837–106846.
4 A. Eichler, L. Tobler, S. Eyrikh, N. Malygina, T. Papina and M. Schwikowski, *Environ. Sci. Technol.*, 2014, **48**, 2635–2642.
5 R. M. Izatt, S. R. Izatt, R. L. Bruening, N. E. Izatt and B. A. Moyer, *Chem. Soc. Rev.*, 2014, **43**, 2451–2475.
6 Z. Li, J. Chen, H. Guo, X. Fan, Z. Wen, M. H. Yeh, C. Yu, X. Cao and Z. L. Wang, *Adv. Mater.*, 2016, **28**, 2983–2991.
7 J. Tang, B. Mu, M. Zheng and A. Wang, *ACS Sustainable Chem. Eng.*, 2015, **3**, 1125–1135.
8 J. Yang, K. Yu and C. Liu, *J. Hazard. Mater.*, 2017, **321**, 73–80.
9 B. L. Rivas, E. D. Pereira, M. Palencia and J. Sánchez, *Prog. Polym. Sci.*, 2011, **36**, 294–322.
10 S. A. El-Safty, S. Abdellatef, M. Ismael and A. Shahat, *Adv. Healthcare Mater.*, 2013, **2**, 854–862.
11 F. Liu, C. Shan, X. Zhang, Y. Zhang, W. Zhang and B. Pan, *J. Hazard. Mater.*, 2017, **321**, 290–298.
12 D. Nagai, M. Yoshida, T. Kishi, H. Morinaga, Y. Hara, M. Mori, S. Kawakami and K. Inoue, *Chem. Commun.*, 2013, **49**, 6852–6854.
13 M. M. Nasef and O. Güven, *Prog. Polym. Sci.*, 2012, **37**, 1597–1656.
14 J. Zhou, V. W.-C. Chang and A. G. Fane, *Energy Environ. Sci.*, 2011, **4**, 2267–2278.
15 D. Godinho, D. Dias, M. Bernardo, N. Lapa, I. Fonseca, H. Lopes and F. Pinto, *J. Hazard. Mater.*, 2017, **321**, 173–182.
16 M. Liu, B. Zhang, H. Wang, F. Zhao, Y. Chen and Q. Sun, *RSC Adv.*, 2016, **6**, 67057–67071.
17 J. Zhao, Z. Li, J. Wang, Q. Li and X. Wang, *J. Mater. Chem. A*, 2015, **3**, 15124–15132.
18 A. Farrukh, A. Akram, A. Ghaffar, S. Hanif, A. Hamid, H. Duran and B. Yameen, *ACS Appl. Mater. Interfaces*, 2013, **5**, 3784–3793.
19 Z. Sekhavat Pour and M. Ghaemy, *RSC Adv.*, 2015, **5**, 64106–64118.
20 C. Chen, R. Wang, L. Guo, N. Fu, H. Dong and Y. Yuan, *Org. Lett.*, 2011, **13**, 1162–1165.
21 B. Ochiai, T. Ogihara, M. Mashiko and T. Endo, *J. Am. Chem. Soc.*, 2009, **131**, 1636–1637.
22 Y. Ge, D. Xiao, Z. Li and X. Cui, *J. Mater. Chem. A*, 2014, **2**, 2136–2145.
23 C. Gai, Y. Guo, N. Peng, T. Liu and Z. Liu, *RSC Adv.*, 2016, **6**, 53713–53722.
24 F. Di Natale, A. Erto, A. Lancia and D. Musmarra, *J. Hazard. Mater.*, 2015, **281**, 47–55.
25 D. S. Tavares, C. B. Lopes, A. L. Daniel-da-Silva, A. C. Duarte, T. Trindade and E. Pereira, *Chem. Eng. J.*, 2014, **254**, 559–570.
26 P. Z. Ray and H. J. Shipley, *RSC Adv.*, 2015, **5**, 29885–29907.
27 M. M. Khin, A. S. Nair, V. J. Babu, R. Murugan and S. Ramakrishna, *Energy Environ. Sci.*, 2012, **5**, 8075.
28 J. Zhang and Y. Chen, *RSC Adv.*, 2016, **6**, 69370–69380.
29 H. Gao, Y. Sun, J. Zhou, R. Xu and H. Duan, *ACS Appl. Mater. Interfaces*, 2013, **5**, 425–432.
30 M. Y. Nassar and S. Abdallah, *RSC Adv.*, 2016, **6**, 84050–84067.
31 F. Perreault, A. Fonseca de Faria and M. Elimelech, *Chem. Soc. Rev.*, 2015, **44**, 5861–5896.
32 J. J. Alcaraz-Espinoza, A. E. Chávez-Guajardo, J. C. Medina-Llamas, C. A. Andrade and C. P. de Melo, *ACS Appl. Mater. Interfaces*, 2015, **7**, 7231–7240.
33 N. Zhang, G. L. Zang, C. Shi, H. Q. Yu and G. P. Sheng, *J. Hazard. Mater.*, 2016, **316**, 11–18.
34 D. Yang, X. Pang, Y. He, Y. Wang, G. Chen, W. Wang and Z. Lin, *Angew. Chem., Int. Ed.*, 2015, **54**, 12091–12096.
35 D. Zheng, X. Pang, M. Wang, Y. He, C. Lin and Z. Lin, *Chem. Mater.*, 2015, **27**, 5271–5278.

36 X.-Q. Liu, Y.-L. Li, Y.-W. Lin, S. Yang, X.-F. Guo, Y. Li, J. Yang and E.-Q. Chen, *Macromolecules*, 2013, **46**, 8479–8487.
37 D. Kundu, C. Hazra, A. Chatterjee, A. Chaudhari, S. Mishra, A. Kharat and K. Kharat, *RSC Adv.*, 2016, **6**, 80438–80454.
38 W. Hu, Y. Liu, T. Chen, Y. Liu and C. M. Li, *Adv. Mater.*, 2015, **27**, 181–185.
39 W. Mai, B. Sun, L. Chen, F. Xu, H. Liu, Y. Liang, R. Fu, D. Wu and K. Matyjaszewski, *J. Am. Chem. Soc.*, 2015, **137**, 13256–13259.
40 A. F. Hirschbiel, S. Geyer, B. Yameen, A. Welle, P. Nikolov, S. Giselbrecht, S. Scholpp, G. Delaittre and C. Barner-Kowollik, *Adv. Mater.*, 2015, **27**, 2621–2626.
41 Y. Yue, R. T. Mayes, J. Kim, P. F. Fulvio, X. G. Sun, C. Tsouris, J. Chen, S. Brown and S. Dai, *Angew. Chem., Int. Ed.*, 2013, **52**, 13458–13462.
42 S. Yuan, J. Gu, Y. Zheng, W. Jiang, B. Liang and S. O. Pehkonen, *J. Mater. Chem. A*, 2015, **3**, 4620–4636.
43 Y. Chen, M. He, C. Wang and Y. Wei, *J. Mater. Chem. A*, 2014, **2**, 10444.
44 M. Cvek, M. Mrlik, M. Ilcikova, T. Plachy, M. Sedlacik, J. Mosnacek and V. Pavlinek, *J. Mater. Chem. C*, 2015, **3**, 4646–4656.
45 J. Pan, J. Zeng, Q. Cao, H. Gao, Y. Gen, Y. Peng, X. Dai and Y. Yan, *Chem. Eng. J.*, 2016, **284**, 1361–1372.
46 B. Ernould, M. Devos, J.-P. Bourgeois, J. Rolland, A. Vlad and J.-F. Gohy, *J. Mater. Chem. A*, 2015, **3**, 8832–8839.
47 J. M. Bak and H.-I. Lee, *Polymer*, 2012, **53**, 4955–4960.
48 J. Luo, F. Zhao, X. Fei, X. Liu and J. Liu, *Chem. Eng. J.*, 2016, **293**, 171–181.
49 S. G. J. Emmerling, L. B. N. Langer, S. A. Pihan, P. Lellig and J. S. Gutmann, *Macromolecules*, 2010, **43**, 5033–5042.
50 S. Banerjee, T. K. Paira, A. Kotal and T. K. Mandal, *Adv. Funct. Mater.*, 2012, **22**, 4751–4762.
51 G. Yin, D. Zhao, L. Zhang, Y. Ren, S. Ji, H. Tang, Z. Zhou and Q. Li, *Chem. Eng. J.*, 2016, **302**, 1–11.
52 N. R. Ko, G. Sabbatier, A. Cunningham, G. Laroche and J. K. Oh, *Macromol. Rapid Commun.*, 2014, **35**, 447–453.
53 X. Wang, J. Cai, Y. Zhang, L. Li, L. Jiang and C. Wang, *J. Mater. Chem. A*, 2015, **3**, 11796–11800.
54 A. S. Krishna Kumar, S.-J. Jiang and W.-L. Tseng, *J. Mater. Chem. A*, 2015, **3**, 7044–7057.
55 E. R. Nightingale, *J. Phys. Chem.*, 1959, **63**, 1381–1387.
56 L. Wang, C. Cheng, S. Tapas, J. Lei, M. Matsuoka, J. Zhang and F. Zhang, *J. Mater. Chem. A*, 2015, **3**, 13357–13364.
57 X. Jing, F. Liu, X. Yang, P. Ling, L. Li, C. Long and A. Li, *J. Hazard. Mater.*, 2009, **167**, 589–596.
58 X. Wang, S. Jing, X. Qiu, S. Zhao, Y. Liu and Y. Tan, *Chem. Eng. J.*, 2016, **304**, 493–502.
59 M. L. Rahman, S. M. Sarkar, M. M. Yusoff and M. H. Abdullah, *RSC Adv.*, 2016, **6**, 745–757.
60 J. Ma, Y. Shen, C. Shen, Y. Wen and W. Liu, *Chem. Eng. J.*, 2014, **248**, 98–106.
61 W. Liu, D. Wei, J. Mi, Y. Shen, B. Cui and C. Han, *Chem. Eng. J.*, 2015, **277**, 312–317.
62 P. Tan, J. Sun, Y. Hu, Z. Fang, Q. Bi, Y. Chen and J. Cheng, *J. Hazard. Mater.*, 2015, **297**, 251–260.
63 P. Tan, J. Wen, Y. Hu and X. Tan, *RSC Adv.*, 2016, **6**, 79641–79650.
64 I. E. M. Carpio, J. D. Mangadlao, H. N. Nguyen, R. C. Advincula and D. F. Rodrigues, *Carbon*, 2014, **77**, 289–301.
65 Q. Zhu and Z. Li, *Chem. Eng. J.*, 2015, **281**, 69–80.
66 D. Liu, Z. Li, W. Li, Z. Zhong, J. Xu, J. Ren and Z. Ma, *Ind. Eng. Chem. Res.*, 2013, **52**, 11036–11044.
67 H. Chen, X. Wang, J. Li and X. Wang, *J. Mater. Chem. A*, 2015, **3**, 6073–6081.
68 R. Cao Jr, A. Díaz, R. Cao, A. Otero, R. Cea, M. C. Rodríguez-Argüelles and C. Serra, *J. Am. Chem. Soc.*, 2007, **129**, 6927–6930.
69 K. Zargoosh, H. Abedini, A. Abdolmaleki and M. R. Molavian, *Ind. Eng. Chem. Res.*, 2013, **52**, 14944–14954.
70 D. Gao, F. Scholz, H. G. Nothofer, W. E. Ford, U. Scherf, J. M. Wessels, A. Yasuda and F. von Wrochem, *J. Am. Chem. Soc.*, 2011, **133**, 5921–5930.

